Geophysical Research Letters

RESEARCH LETTER
10.1029/2021GL094541

Winter Snow Depth on Arctic Sea Ice From Satellite Radiometer Measurements (2003–2020): Regional Patterns and Trends

Sang-Moo Lee[1,4], Hoyeon Shi[2], Byung-Ju Sohn[2,3], Albin J. Gasiewski[1], Walter N. Meier[4], and Gorm Dybkjær[5]

[1]Center for Environmental Technology, Electrical, Computer, and Energy Engineering, University of Colorado, Boulder, CO, USA, [2]School of Earth and Environmental Sciences, Seoul National University, Seoul, Korea, [3]Key Laboratory for Aerosol-Cloud-Precipitation of China Meteorological Administration, School of Atmospheric Physics, Nanjing University of Information Science and Technology, Nanjing, China, [4]National Snow and Ice Data Center, Cooperative Institute for Research in Environmental Sciences, University of Colorado, Boulder, CO, USA, [5]Danish Meteorological Institute, Copenhagen, Denmark

Key Points:

- Wintertime Arctic basin-scale snow depth on sea ice has been retrieved from satellite radiometer measurements from 2003 to 2020
- Significant snow depth reduction is noted compared to the modified Warren climatological snow depth over the Arctic basin
- Positive trends of snow depth are found over multiyear sea ice areas during the 2003–2020 period

Supporting Information:

Supporting Information may be found in the online version of this article.

Correspondence to:

S.-M. Lee,
Sang-Moo.Lee@colorado.edu;
dr.sangmoolee@gmail.com

Citation:

Lee, S.-M., Shi, H., Sohn, B.-J., Gasiewski, A. J., Meier, W. N., & Dybkjær, G. (2021). Winter snow depth on Arctic sea ice from satellite radiometer measurements (2003–2020): Regional patterns and trends. *Geophysical Research Letters*, *48*, e2021GL094541. https://doi.org/10.1029/2021GL094541

Received 4 JUN 2021
Accepted 26 JUL 2021

Abstract Retrieval of snow depth on sea ice from satellite measurements has been challenging especially for multiyear ice. In this study, January-February-March monthly averaged snow depth was estimated during the 2003–2020 period from satellite radiometer measurements by combining recently developed retrieval methods for freeboard and snow-ice thickness ratio. A good agreement between snow depth from this study and that from Operational IceBridge measurements demonstrates that reliable snow depth can be estimated from satellite measurements. From the analysis of wintertime snow depth estimated from this study, a reduction of mean snow depth compared to the modified Warren climatology is noted over the entire Arctic Ocean. In addition, this study found geographically different snow depth trends: positive for multiyear ice area and negative for the other areas. Average snow depth interannual variability on multiyear ice ranges between 3 to 5 cm while smaller variability is found on first-year ice.

Plain Language Summary Snow on Arctic sea ice plays an important role in the Arctic surface energy balance and hydrological cycle. In this study, the snow depth on Arctic sea ice is retrieved based on the satellite measurements during the January-February-March months of the 2003–2020 period. We found a good agreement between snow depth from this study and snow depth measurements from airborne snow radar. Analysis of the mean and trend of snow depth demonstrates that the reduction of snow depth on sea ice occurs in the whole Arctic area compared to the climatological values measured during 1954–1991. In the Eastern and Western Arctic Ocean, there are significant decreasing and increasing snow depth trends, respectively.

1. Introduction

While an unambiguous climate change signature has been observed in Arctic sea ice coverage (Andersen et al., 2020; Stroeve et al., 2007), it has been difficult to quantify the changes in snow depth over the sea ice region (Webster et al., 2018). This holds in spite of snow accumulation being one of the most important geophysical parameters to understand Arctic climate, being related to albedo feedback, ice cover insulation, and associated heat transfer effects (Curry et al., 1995; Ledley, 1991; Webster et al., 2014). In addition to its importance in the polar climate system, snow depth influences the accuracy of ice thickness estimation based on satellite altimetry (Kern et al., 2015). Most knowledge regarding snow depth on Arctic sea ice is based on the climatological distribution provided by Warren et al. (1999) (W99), which was based on in situ data collected over multiyear sea ice (MYI) during the years of 1954–1991. Although W99 may not be considered as a representative Arctic snow depth distribution for the recent decades, it is still often used as a standard. For example, based on a report by Kurtz and Farrell (2011), many studies modified W99 by halving W99 snow depth over first-year ice (FYI), then using this scaled snow depth to estimate ice thickness from satellite altimeter measurements (Kwok & Cunningham, 2015; Ricker et al., 2014). A reliable data record of the snow depth is thus clearly needed by both climate and satellite communities (Webster et al., 2014).

A commonly referenced retrieval method for Arctic basin-scale snow depth from satellite passive microwave (PMW) measurements uses the gradient ratio (GR) defined as a normalized difference in *p*-polarized brightness temperatures (TB) at two frequencies (Markus & Cavalieri, 1998). Initially, algorithm availability was restricted to FYI, until a recent study extended the GR-based method to estimate snow depth on MYI by using the lower microwave frequency of 6.925 GHz (Rostosky et al., 2018; hereafter referred to as the 'improved GR-method'). In either case, the GR-based method has a large sensitivity to surface geometric tilt (Lee et al., 2018; Stroeve et al., 2006). Additionally, the improved GR-method was trained with snow depth measurements from Operation IceBridge (OIB), which covers a limited area during March and April. Thus, even the improved GR-method on MYI is limited to the spring season. Other efforts to reconstruct snow depth distributions are based on modeling approaches (Liston et al., 2020; Petty et al., 2018). These results are highly reliant upon the reanalysis data set, which have high uncertainties in snowfall rates across the Arctic (Boisvert et al., 2018; Lindsay et al., 2013).

A recent study demonstrated that it is theoretically possible to estimate ice freeboard (i.e., distance from the sea surface to the snow-ice interface) from PMW measurements by relating the physical depth (ice freeboard) to the snow-ice scattering optical depth (SOD) caused by snow and freeboard scatterings (Lee et al., 2021). Additionally, it has been demonstrated that snow depth can be retrieved with high accuracy by combining the freeboard measurements with the ratio of snow depth to ice thickness (Shi et al., 2020).

In this study, we attempt to estimate Arctic basin-scale snow depth by combining the freeboard retrieval method of Lee et al. (2021) and the snow depth retrieval method of Shi et al. (2020) and applying this method to satellite data from the Advanced Microwave Scanning Radiometer (AMSR)-E and AMSR2. Estimated snow depths using this method are validated against OIB measurements. In addition, this study provides mean and standard deviation (STD) fields of snow depth, which can be used as an alternative snow depth input for satellite altimetry. Additionally, we present trends in snow depth over the AMSR period (2003–2020), showing that trends in snow depth are negative over regions where ice type transitions from MYI to FYI occur and positive over MYI.

2. Data

In this study, daily AMSR-E and AMSR2 TB fields on 25-km polar stereographic grid at 6.925, 10.65, 18.7, and 36.5 GHz for January-February-March (JFM) months of 2003–2020 are used to retrieve the Snow-Ice Interface Temperature (SIIT; Lee & Sohn, 2015), SOD (Lee et al., 2021), and ice type (Lee et al., 2017). There is a data gap in 2012 because AMSR-E was not operational that year. Top-of-atmosphere TB fields are converted into values at the snow surface by correcting for atmospheric influences, which are calculated using the Satellite Data Simulator Unit (Masunaga et al., 2010) with inputs from the European Centre for Medium-Range Weather Forecast ReAnalysis-5th Generation (ERA5; Hersbach et al., 2020). To intercalibrate AMSR-E and AMSR2 TBs, AMSR2 TBs are converted into AMSR-E-equivalent TBs based on the inter-calibration coefficients introduced from JAXA (2015). Data that is distant from coastlines by less than 100-km is discarded to prevent land contamination effects due to the large footprint of PMW observation, which can cause systematic errors in retrievals (Cavalieri et al., 1999). The retrievals are done only over the area where the sea ice concentration (SIC) is greater than 98% to avoid the ocean contamination. Daily gridded 25-km SIC data from the "NOAA/NSIDC Climate Data Record of Passive Microwave Sea Ice Concentration-Version 3" data set is used (Meier, Fetterer, Savoie, et al., 2017), and a near-real-time version of the CDR data are used for 2020 (Meier, Fetterer, & Windnagel, 2017).

ICESat and ICESat-2 total freeboard F_t (i.e., distance from the sea surface to snow surface) is used for relating the SOD to F_t. Both are satellite laser altimeters which measure the F_t by analyzing signal reflected at snow or sea surface. For ICESat data, along-track F_t measurements included in the "Arctic Sea Ice Freeboard and Thickness-Version 1" data set (Yi & Zwally, 2009) are used and re-gridded on a 25-km grid. Since ICESat measurements are not available for January, daily F_t data were prepared for all available February-March months of 2003–2008. For ICESat-2, daily gridded F_t on a 25-km grid included in the "ATLAS/ICESat-2-L3B Daily and Monthly Gridded Sea Ice Freeboard-Version 1" data set (Petty, Kwok, et al., 2020) is used over JFM months during 2019–2020.

To obtain the snow depth h_s to ice thickness H_i ratio (hereafter referred to as α), monthly averaged Snow Top Temperature (STT) is required. STT data for the 2017–2020 period are obtained from the "High Latitude-L2 Sea and Sea Ice Surface Temperature (OSI-205-a)" data set (Dybkjær, Eastwood, Borg, et al., 2018) distributed by Ocean and Sea Ice-SAF (OSI-SAF). The OSI-205-a product was derived from Advanced Very High-Resolution Radiometer (AVHRR) TBs at 3.74, 10.8, and 12.0 μm using the split-window algorithm (Dybkjær, Eastwood, & Howe, 2018). Only data flagged at quality level of 'acceptable' or 'excellent' are kept and re-gridded on the 25-km grid. For the 2003–2015 period, the data are obtained from the Arctic and Antarctic ice Surface Temperatures from thermal Infrared satellites sensors-version 2 (AASTI-v2) data set (Dybkjær et al., 2014). Because AASTI-v2 is derived from AVHRR TBs using the same algorithm as OSI-205-a, those two datasets are assumed consistent STT records for 2003–2020. It is noted that STT data are not available for 2016. Daily AASTI-v2 data in a 0.25° grid format are re-gridded to the 25-km grid. Finally, monthly fields of STT are obtained by averaging daily fields under the condition of SIC greater than 98%.

OIB-measured F_t and h_s (Koenig et al., 2010) are used as a reference for independently evaluating the here derived products. NASA's OIB, which is an aircraft mission, measures both F_t and h_s over the Arctic Ocean using a snow radar and lidar (Airborne Topographic Mapper) (N. T. Kurtz et al., 2013). These instruments were functional during the 2009–2018 OIB Arctic flights. The 2009–2013 period data are obtained from the "IceBridge-L4 Sea Ice Freeboard, Snow Depth, and Thickness-Version 1" data set (N. Kurtz et al., 2015), and the 2014–2018 period data are obtained from the quick-look data set distributed at the NSIDC (https://doi.org/10.5067/GRIXZ91DE0L9). The OIB data are collocated on the 25-km grid by averaging the nearest OIB observations to the grid point.

To make a comparison between our results and other products, modified W99 (i.e., mW99) and reanalysis-based h_s modeling (SnowModel-LG; Liston et al., 2020) data are introduced. Daily fields of mW99 are obtained by halving W99 over the FYI region using ice type derived from AMSR measurements (Lee et al., 2017). SnowModel-LG accumulates and redistributes snowfall from atmospheric reanalysis in a Lagrangian framework using ice motion vectors (Liston et al., 2020). This study utilizes daily h_s fields of SnowModel-LG forced with ERA5 and ice motion vectors from Tschudi et al. (2019). The SnowModel-LG data are available up to 2018.

3. Methods

In this study, daily AMSR TBs are used to estimate SOD. The daily estimated SODs are regressed to the ICESat and ICESat-2 F_t. The daily estimated F_t fields from SOD are monthly averaged to use the method described below (referred to as the α-method) for estimating h_s. A detailed explanation for h_s estimation is provided below.

A recent study by Shi et al. (2020) developed an algorithm to estimate h_s by combining the F_t measured by satellite altimetry with the ratio α between h_s and H_i (i.e., $\alpha \equiv h_s/H_i$). Introducing the definition of α, the hydrostatic balance equation can be expressed for h_s as:

$$h_s = \frac{\alpha \rho_w}{\rho_w - \rho_i + \alpha\left(\rho_w - \rho_s\right)} F_t \tag{1}$$

where ρ_w, ρ_i, and ρ_s denote the bulk densities of water, ice, and snow, respectively. The bulk densities used in this study are 320 and 1024 kg/m^3 for snow and water, respectively. We assume that ρ_i is 915 kg/m^3 regardless of ice type because of the following two reasons: (1) the h_s uncertainty due to ρ_i is minor, (2) 915 kg/m^3 is generally accepted in satellite and airborne altimetry application (Kurtz & Harbeck, 2017; N. T. Kurtz et al., 2013; Petty, Kurtz, et al., 2020). The detailed discussions regarding ρ_i can be found in Text S1.

Based on the analysis of buoy-measured temperature profiles by Shi et al. (2020), we assume that the monthly averaged temperature profile within the snow and ice layers is linear during winter. Therefore, the ratio α can be expressed as the ratio of the temperature difference in the snow layer (i.e., STT minus SIIT) to the temperature difference in the ice layer (i.e., SIIT minus the ice bottom temperature) under the assumption that conductive heat flux is continuous at the snow-ice interface (Maykut & Untersteiner, 1971). It was found that α and the temperature difference ratio follow piecewise linear relationships when monthly averaged thicknesses and temperatures from 12 buoy measurements covering the 1998 and 2010–2014 periods

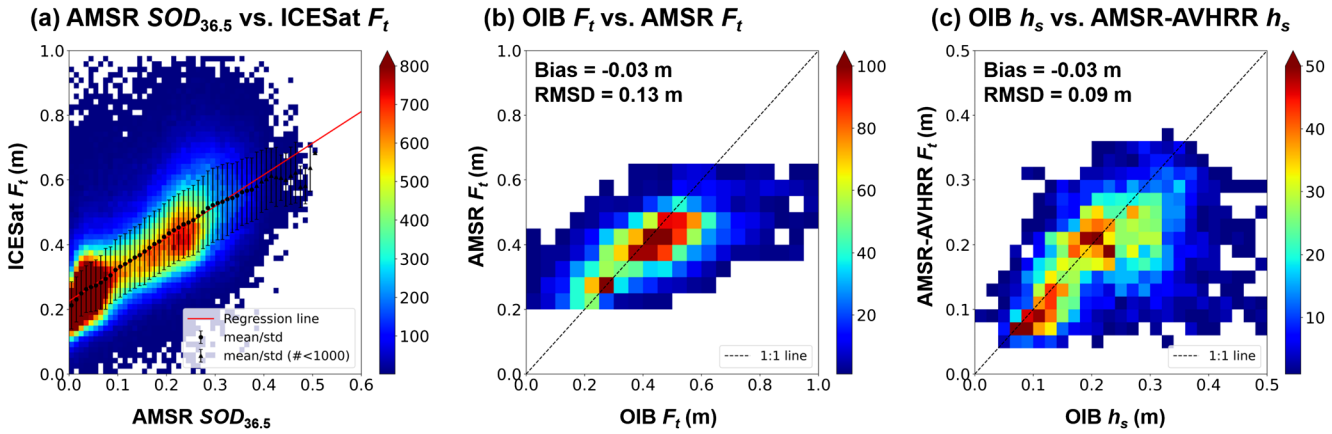

Figure 1. (a) Two-dimensional histogram between Advanced Microwave Scanning Radiometer (AMSR) scattering optical depth at 36.5 GHz $SOD_{36.5}$ and ICESat F_t. Mean and standard deviation at every 0.01 bin of $SOD_{36.5}$ are overlayed. The comparison period is the January-February-March (JFM) months of 2003–2008 (ICESat) and 2019–2020 (ICESat-2). (b) Validation results of AMSR-estimated daily F_t with respect to Operation IceBridge (OIB)-measured one during March 2009–2018. (c) Validation results of AMSR-AVHRR derived monthly h_s with respect to OIB-measured daily h_s during March 2009–2018.

were analyzed (Shi et al., 2020). Since these relationships showed a time-invariant nature, an "α-prediction equation," which is an empirical relation between α, STT, SIIT, and ice bottom temperature, was obtained to estimate α from satellite-derived STT and SIIT. The α-prediction equation and coefficients can be found in Equation 15 and Table 2 of Shi et al. (2020). Ice bottom temperature is fixed at −1.5°C (Shi et al., 2020). Finally, monthly fields of α are obtained from monthly averaged STT and SIIT data. Therefore, once the F_t is known, the h_s can be estimated using Equation 1 with the measured α.

Lee et al. (2021) suggested an algorithm for SOD retrieval from satellite PMW measurements by solving a simplified sea ice radiative transfer equation with an assumption that the emitting layer temperature and refractive index of sea ice are frequency-independent between 6.9 and 36.5 GHz. The detailed methodology for estimating SOD is given in Lee et al. (2021). Since SOD is proportional to the physical thickness of freeboard ice and snow layers by definition of optical depth, F_t can be estimated by relating the SOD to F_t obtained from ICESat and ICESat-2. While Lee et al. (2021) used radar-measured ice freeboard, this study uses lidar-measured F_t because the h_s estimates based on the α-method are more accurate when F_t is used rather than ice freeboard (Shi et al., 2020).

Figure 1a shows the two-dimensional scatterplot between SOD at 36.5 GHz (i.e., $SOD_{36.5}$) and F_t. Since most of the data pairs congregate on the small values of both SOD and F_t, instead of deriving a relationship directly from the scatterplot of Figure 1a, we consider a binned analysis for estimating fitting coefficients. Since binning data leads to a loss of information because this method only uses mean value of each bin and does not consider its variance, we introduce the weighted least square fit to incorporate the variance of F_t into the regression in order to minimize loss of data information. This fitting approach better accounts for the smaller density of larger SOD and F_t values than linear least square fitting, and thus, precludes a regression dominated by lower SOD and F_t values. Additionally, if the number of F_t is less than 1000 in a certain bin, the corresponding bin is omitted. The resulting fit is:

$$F_t = (0.98) SOD_{36.5} + 0.23 \quad (2)$$

According to Equation 2, there is a lower limit of F_t retrieval from SOD. Therefore, this approach has limitation on F_t estimation less than 0.2 m. Although we found that fully concentrated winter ice area generally has F_t greater than 0.2 m, the retrievals of h_s is possibly overestimated over areas having F_t less than 0.2 m. The regressed F_t is validated with OIB-measured F_t, indicating that the AMSR-estimated F_t is in good agreement with OIB F_t with a small bias of −0.03 m and RMSD of 0.13 m (Figure 1b).

Once F_t is estimated, the h_s can be estimated using Equation 1 along with the estimated α. In this study, monthly averages of daily AMSR-estimated F_t fields were used as input for Equation 1. The estimated h_s is validated against OIB-measured h_s (Figure 1c). The resulting statistics are a bias of −0.03 m and RMSD of 0.09 m.

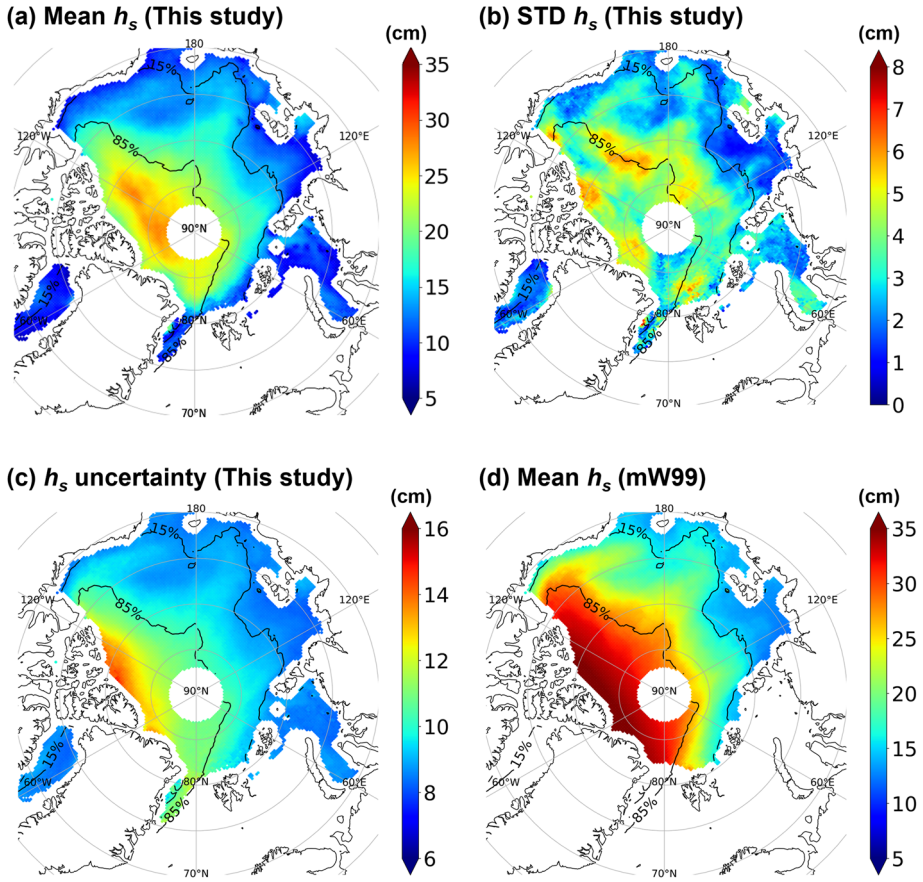

Figure 2. (a) Mean and (b) detrended standard deviation fields of January-February-March (JFM)-averaged h_s from this study over the 2003–2020 period. (c) JFM-averaged total uncertainties of the estimated h_s due to input parameters. (d) Mean field of JFM-averaged h_s from mW99 climatology over the 2003–2020 period. The contours indicate the multiyear sea ice (MYI) data frequency during the study period.

The uncertainties in h_s induced by each input parameter (i.e., α, F_t, ρ_i, and ρ_s) are calculated using the method described in Text S2 and illustrated in Figure S1. It is revealed that there are two major contributors of α and F_t to h_s uncertainties. It is interesting to note that α is the main uncertainty contributor to uncertainty in h_s over the north of the Canadian Archipelago-Greenland coasts while F_t contributes nearly uniform uncertainty in h_s of 8 cm over the entire Arctic Ocean. The contribution of ρ_i and ρ_s to the total uncertainty of h_s is low compared to the contribution of α and F_t. Total uncertainties of h_s retrievals can be estimated using the Gaussian error propagation model (Text S2) and illustrated in Figure 2c. The total h_s uncertainty ranges from 8 to 15 cm.

Additionally, we provide an algorithm sensitivity test to the two major input variables of α and F_t for the reference states (The details are provided in Text S2). The sensitivity test shows that $\pm$10% errors in α can bring about $\sim\pm$1 cm error in h_s estimates which corresponds to $\sim\pm$6% of reference h_s. In the case of F_t, the $\pm$10% error in F_t can cause to $\sim\pm$1.5 cm error which corresponds to $\sim\pm$10% of the reference h_s.

4. Results

4.1. Geographical Distribution of Mean Snow Depth

Based on the procedures described in Section 3, the spatial distributions of h_s are obtained for the JFM months of the 2003–2020 period (Figure S2). The 17-year mean spatial distribution of winter h_s is illustrated in Figure 2a. There are two year-long data gaps (i.e., 2012 and 2016) as mentioned in Section 2. The deepest snow is noted over the north of Greenland and the Canadian Archipelago where MYI is prevalent and is

between 16.5 and 28.2 cm, while a low snow depth is observed over the north of the Canadian Archipelago. The farther away from the Central Arctic, the thinner h_s tends to be. The lowest mean h_s is found in the Kara and Laptev Seas, ranging from 6.8 to 16.1 cm.

In order to consider the rapid decline in MYI area over the study period, we define a "MYI area" as pixels where the MYI frequency (i.e., defined as the portion of MYI flag within pixel during the analysis period) is greater than 85% and a "FYI area" as pixel where the MYI frequency is less than 15%. The rest is defined as a "mixed area". In general, h_s over the MYI area is found to be deeper than over the FYI area because the snow accumulation period is longer on MYI. This is also seen in other model-based and satellite-based h_s products (Rostosky et al., 2018; Zhou et al., 2021). The overall mean h_s distribution is generally consistent with mW99 (Figure 2d). However, h_s values obtained from this study are found to be lower than mW99, showing a large discrepancy over the Beaufort Sea where most of the ice type turns into FYI (also see Figure S3a). Geographical differences between h_s from this study and SnowModel-LG are described in Figure S3 and Text S3.

The distributions of STD fields from time-detrended h_s anomalies (i.e., interannual variability) are plotted in Figure 2b. It is noted that STD distributions are generally proportional to the mean fields except for the areas with the deepest snow over Central Arctic. The highest values are found over the mixed area which is likely associated with ice type transitions. It is observed that the interannual variabilities of JFM h_s on the MYI area are generally between 3 and 5 cm, which is larger than that on FYI area. The range of JFM h_s variability on the MYI areas lies between previously reported values from W99 (4.6–6.2 cm) while snow accumulation models reported values from 2 to 3 cm (Zhou et al., 2021).

4.2. Temporal Variation of Snow Depth on Arctic Sea Ice

The available winter mean h_s estimates over the study period provide an opportunity to address two important questions of (a) how has wintertime h_s changed over the Arctic basin during this period? and (b) how does this the time variation of h_s differ from region to region? To answer these questions general trends of h_s and associated time series are presented in Figure 3. The results obtained indicate that h_s trends are highly spatially variable over the Arctic basin. Statistically significant (i.e., $p < 0.05$) positive trends in h_s of $\sim$+0.6 cm/yr on average are observed over MYI (Figure 3a). Most of the significant negative trends fall into the mixed area where ice type transitions occur ($\sim$−0.4 cm/yr on average). Over the remaining FYI areas, the trends are insignificant except for the Laptev Sea where significant negative trends are noted. Such regionally different trends of h_s are also noted for each JFM month (Figure S4).

Since snowfall on sea ice is closely related to Arctic cyclone activity (Serreze et al., 2012), the positive trend is possibly related to increased autumn and winter precipitation, which is likely caused by more enhanced and westward Arctic cyclone activity (Kenigson & Timmermans, 2021). SnowModel-LG shows a similar spatial distribution of h_s trends but with stronger negative trends over FYI and mixed areas and with less organized positive trends over MYI area (Figure 3c). However, over a longer period from 1991 to 2015, reanalysis-based h_s data set show significant positive h_s trends on MYI over the north of Canadian Archipelago (Zhou et al., 2021), in agreement with this study. It is interesting to note that this positive h_s trend is hardly found in the improved GR-method (Figure S5a). The decreasing trends in h_s over FYI could be related to the precipitation phase and freeze-up date (Webster et al., 2018). As delayed freeze-up dates due to an Arctic warming shortens the period of snow accumulation, consequently h_s on FYI would be reduced in recent years. For h_s over the mixed area, negative trends of h_s are well corresponding to the decreasing trends of MYI frequency (Figure 3a), implying that ice type changes are responsible for the h_s reduction as well. Such negative trends are also found in SnowModel-LG data (Figure 3b) and the improved GR-method (Figure S5a). Compared to the mW99 climatology (1954–1991 period), it is found that the recent JFM Arctic mean h_s from both this study and SnowModel-LG have become $\sim$30% thinner.

From the mean Arctic basin-scale point of view, the overall trend in h_s appears less distinct than the regional trends during the recent 18 years (Figure 3e). However, it is noted that the h_s distribution has undergone significant regional changes over this period. Figure 3c shows the probability distribution functions (PDFs) of h_s for 2003–2020. For the earlier period (2003–2007), the distribution is bimodal with peaks in h_s at 12.5 and 23 cm. These two peaks correspond to the h_s on FYI and MYI, respectively (see Figure 3d). In contrast, the h_s distribution in the later period (2017–2020) shows only a single peak at 13 cm. PDFs for each year can

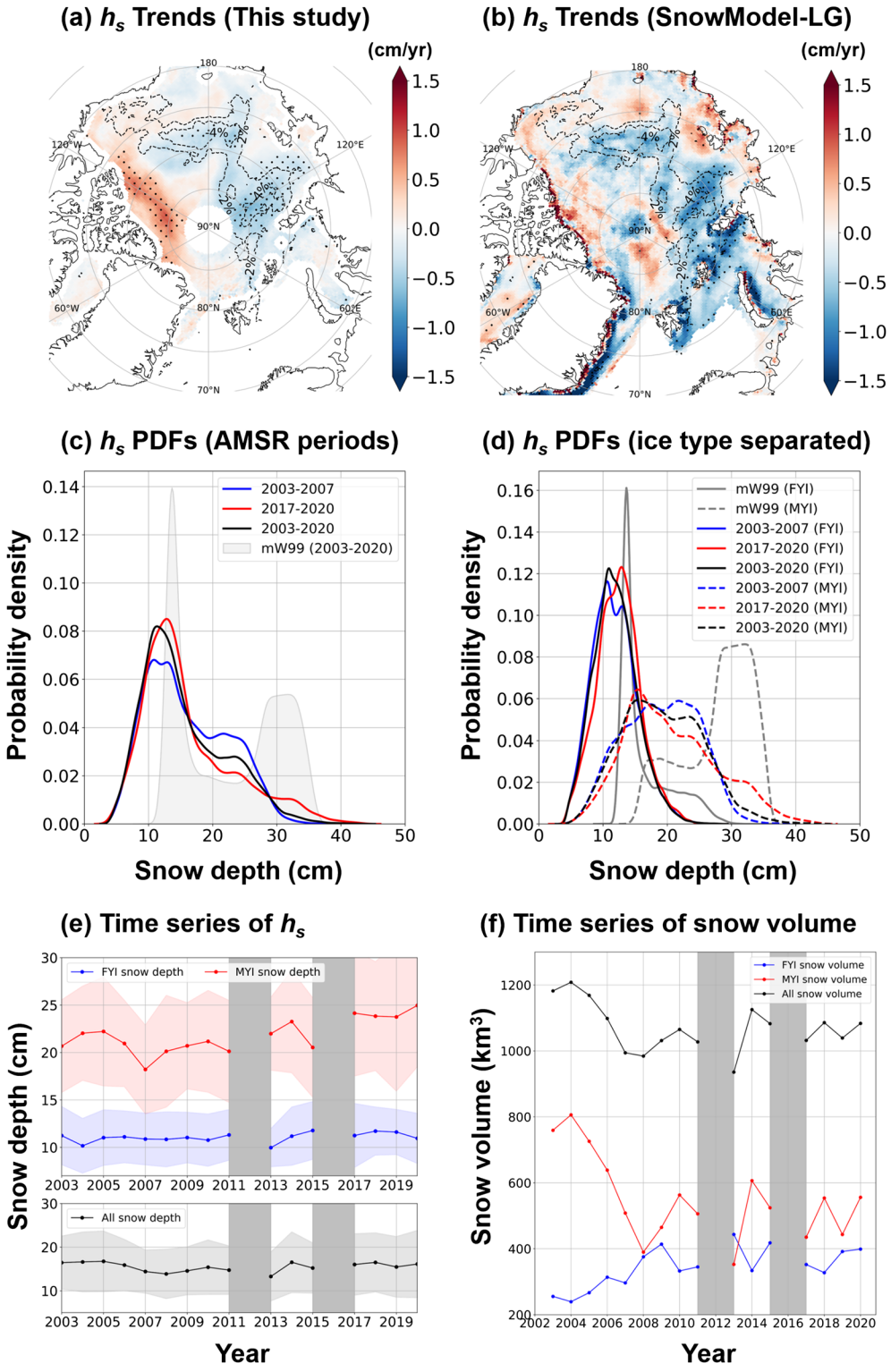

Figure 3. Trends of January-February-March (JFM)-averaged h_s from (a) this study (2003–2020) and (b) the SnowModel-LG (2003–2018). The contours in (a) and (b) indicate the trend of multiyear sea ice (MYI) data frequency. (c) Probability distribution functions (PDFs) for JFM-averaged h_s and (d) PDFs separated over each ice types during three different periods, along with mW99 PDFs. Time series of (e) mean h_s, and (f) snow volumes from this study.

be found in Figure S6. These PDFs suggest that in more recent years the h_s on FYI has become the dominant contributor to the overall h_s over the Arctic basin. Because of this, the net snow volume is trending to be slightly negative despite the MYI h_s trending to be positive (Figure 3f). These conclusions are consistent with recent trends in sea ice coverage where FYI is becoming a larger fraction of overall coverage (Andersen et al., 2020).

5. Summary and Discussions

Winter Arctic basin-scale h_s was estimated for the 2003–2020 period using satellite radiometer measurements along with a physics-based algorithms. Most of the h_s retrievals rely upon OIB products showing differences from product to product (Kwok et al., 2017), which implies the OIB-dependent h_s should inherit potential bias within certain OIB products. On the other hand, h_s data record provided by this study is a unique data set because the suggested h_s estimation method is independent of OIB measurements. Although the suggested method is independent from OIB data, a good consistency in h_s between this study and OIB (N. Kurtz et al., 2015) was found. It demonstrates that a reliable h_s can be estimated from satellite radiometer measurements.

The estimated basin-averaged h_s is ∼30% thinner than mW99 values during the winter months. From the mean Arctic basin-scale point of view, the overall trend in h_s appeared less distinct than the regional trends during the 2003–2020 period. However, it is noted that the h_s distribution has undergone significant regional changes over this period. Statistically significant positive trends are found over MYI (∼0.6 cm/yr on average) and negative over mixed/FYI areas (∼−0.4 cm/yr on average). These trends were also observed in SnowModel-LG. Consequences and implications of the observed results for Arctic remote sensing and climate studies are as follows.

It has been suggested that mW99 introduces systematic bias in H_i retrieval using satellite altimetry (Kwok et al., 2020). The present study further substantiates that the mean h_s is significantly reduced compared to the mW99 for both ice types. This has been reported by other researchers (Kwok et al., 2020; Rostosky et al., 2018), as well. The overestimated mW99 h_s will likely cause underestimation of H_i when using lidar, and overestimation when using radar to estimate sea ice thickness (Shi et al., 2020). Such systematic bias due to mW99 can in turn cause a significant bias between H_is estimated from lidar and radar altimeters (Kim et al., 2020). Additionally, the regional trends of h_s revealed in this study suggest that altimeter-derived H_i trends using the mW99 climatology most likely produce erroneous regional trends in the derived H_i due to neglect of these h_s trends (Bunzel et al., 2018). In conclusion, time dependent h_s data should be preferred over mW99 for more accurate H_i retrieval. In addition, time-dependent h_s product can be used to investigate the impact of overestimated h_s on H_i retrievals.

The observed Arctic basin-scale h_s records from this study can be used for improving the atmospheric states of reanalysis data and thus Arctic climate prediction. Most Arctic climate studies utilize reanalysis fields due to the general lack of available observations over the Arctic. For example, anomalous surface turbulent heat flux was used as an indicator to investigate causality between sea ice reduction and midlatitude cold winter (Blackport et al., 2019). However, most atmospheric reanalysis models neglect snow on sea ice even if it is a crucial parameter to determine surface energy balance (Batrak & Müller, 2019; ECMWF, 2007, 2016). The conductive heat flux is balanced with other energy fluxes above the snow surface, such as upwelling/downwelling longwave radiation and turbulent heat fluxes. Lack of snow information may lead to conductive heat flux being overestimated, resulting in a warm bias of STT (Batrak & Müller, 2019; Wang et al., 2019). Reanalysis models should consider regional h_ss to provide more realistic surface energy fluxes for climate studies and require the assimilation of appropriate h_s. Similarly, climate models require realistic initial conditions for improved climate prediction. The h_s records in this study should be valuable for such purposes.

Since the main contributors to h_s uncertainties are α and F_t, the expected uncertainties in h_s can be reduced with extensive analysis for buoy measurements for precisely modeling the α- and F_t-prediction equations. The inclusion of additional buoy measurements for improving the α-prediction equation, the advance of satellite temperature retrieval algorithms, and the advance of the F_t retrieval algorithm can reduce uncertainties in the h_s estimation.

Data Availability Statement

Monthly snow depth data produced in this study and the associated monthly uncertainty estimates are available at the Zenodo data repository (https://doi.org/10.5281/zenodo.5081765). AMSR TB data are available from both the JAXA ftp repository (AMSR-E: ftp://ftp.gportal.jaxa.jp/standard/AQUA/AQUA.AMSR-E) (AMSR2: ftp://ftp.gportal.jaxa.jp/standard/GCOM-W/GCOM-W.AMSR2) and G-portal website (https://gportal.jaxa.jp/gpr/search?tab=1), and user registration is required through the website (https://gportal.jaxa.jp/) to access the data. ERA5 data are available at the Copernicus Climate Change Service (C3S) Climate Data Store (https://doi.org/10.24381/cds.bd0915c6). SIC, ICESat, and OIB data are available at the NSIDC website (SIC CDR: https://doi.org/10.7265/N59P2ZTG; Near-real-time SIC CDR: https://doi.org/10.7265/N5FF3QJ6; ICESat: https://doi.org/10.5067/SXJVJ3A2XIZT; ICESat-2: https://nsidc.org/data/ATL20/versions/1; OIB L4: https://doi.org/10.5067/G519SHCKWQV6; OIB Quick Look: https://doi.org/10.5067/GRIXZ91DE0L9). For STT data, the OSI-205-a product is available at the OSI SAF website (http://osisaf.met.no/p/ice/sst-ist-l2.html). AASTI data with resolution of 0.05° is available at Copernicus Marine Service website in NetCDF format (https://resources.marine.copernicus.eu/?option=com_csw&view=details&product_id=SEAICE_ARC_PHY_CLIMATE_L4_MY_011_016). Snow depth data from the improved GR-method is available at the PANGAEA repository (AMSR-E: https://doi.org/10.1594/PANGAEA.902748; AMSR2: https://doi.org/10.1594/PANGAEA.902747). SnowModel-LG data are available at the NSIDC website (https://doi.org/10.5067/27A0P5M6LZBI).

Acknowledgments
The authors would like to thank two anonymous reviewers for their constructive and valuable comments that led to an improved research article. The first two authors (Sang-Moo Lee and Hoyeon Shi) are co-lead authors and each contributed equally to the manuscript. The other authors (Sohn, Gasiewski, Meier, and Dybkjær) contributed in lesser roles through providing analysis and interpretation of the data fields, guidance on the focus of the paper, and contributing to the production of the manuscript. The authors appreciate NSIDC for providing the OIB, ICESat, ICESat-2, and SIC datasets, JAXA for providing AMSR-E and AMSR2 TB fields, and ECMWF for providing ERA5 atmospheric fields. This work is supported by a National Research Foundation of Korea (NRF) grant funded by the Korean government (MSIP) (grant ref. no. NRF-2019R1A6A3A03032352), and a grant to the University of Colorado Boulder by Orbital Micro Systems, Inc. The work of Hoyeon Shi and Byung-Ju Sohn is supported by the NRF grant (grant ref. no. NRF-2018M1A3A3A02065661). The authors thank Dr. Liston for sharing the SnowModel-LG snow depth data.

References

Andersen, J. K., Andreassen, L. M., Baker, E. H., Ballinger, T. J., Berner, L. T., Bernhard, G. H., et al. (2020). The Arctic. *Bulletin of the American Meteorological Society*, *101*, S239–S286. https://doi.org/10.1175/BAMS-D-20-0086.1

Batrak, Y., & Müller, M. (2019). On the warm bias in atmospheric reanalyses induced by the missing snow over Arctic sea-ice. *Nature Communications*, *10*, 4170. https://doi.org/10.1038/s41467-019-11975-3

Blackport, R., Screen, J. A., van der Wiel, K., & Bintanja, R. (2019). Minimal influence of reduced Arctic sea ice on coincident cold winters in mid-latitudes. *Nature Climate Change*, *9*, 697–704. https://doi.org/10.1038/s41558-019-0551-4

Boisvert, L., Webster, M., Petty, A., Markus, T., Bromwich, D., & Cullather, R. (2018). Intercomparison of precipitation estimates over the Arctic Ocean and its peripheral seas from reanalyses. *Journal of Climate*, *31*(20), 8441–8462. https://doi.org/10.1175/JCLI-D-18-0125.1

Bunzel, F., Notz, D., & Pedersen, L. T. (2018). Retrievals of Arctic sea-ice volume and its trend significantly affected by interannual snow variability. *Geophysical Research Letters*, *45*, 11751–11759. https://doi.org/10.1029/2018GL078867

Cavalieri, D. J., Parkinson, C. L., Gloersen, P., Comiso, J. C., & Zwally, H. J. (1999). Deriving long-term time series of sea ice cover from satellite passive-microwave multisensory data sets. *Journal of Geophysical Research*, *104*(C7), 15803–15814. https://doi.org/10.1029/1999JC900081

Curry, J. A., Schramm, J. L., & Ebert, E. E. (1995). Sea ice-albedo climate feedback mechanism. *Journal of Climate*, *8*, 240–247. https://doi.org/10.1175/1520-0442(1995)008<0240:SIACFM>2.0.CO;2

Dybkjær, G., Eastwood, S., Borg, A. L., Højer, J., & Tonboe, R. (2018). *Algorithm theoretical basis document for the OSI SAF Sea and Sea Ice Surface Temperature L2 processing chain, OSI-205-a and OSI-205-b, Version 1.4*. OSI SAF. Retrieved from http://osisaf.met.no/p/ice/sst-ist-l2.html

Dybkjær, G., Eastwood, S., & Howe, E. (2018). *OSI SAF high latitudes L2 sea and sea ice surface temperature product user manual, OSI-205-a and OSI-205-b, version 1.3*. OSI SAF. Retrieved from http://osisaf.met.no/p/ice/sst-ist-l2.html

Dybkjær, G., Højer, J., Tonboe, R., & Olsen, S. (2014). Report on the documentation and description of the new Arctic Ocean dataset combining SST and IST. *NACLIM Deliverable*, D32. 28.

European Centre for Medium-range Weather Forecasts (ECMWF). (2007). Part IV: Physical Processes. *IFS Documentation–Cy31r1*. 1–155. https://doi.org/10.21957/orqi6pqsa

European Centre for Medium-range Weather Forecasts (ECMWF). (2016). Part IV: Physical Processes. *IFS Documentation–Cy41r2*. 1–213. https://doi.org/10.21957/tr5rv27xu

Hersbach, H., Bell, B., Berrisford, P., Hirahara, S., Horányi, A., Muñoz Sabater, J., et al. (2020). The ERA5 global reanalysis. *Quarterly Journal of the Royal Meteorological Society*, *146*, 1999–2049. https://doi.org/10.1002/qj.3803

Japan Aerospace Exploration Agency (JAXA). (2015). *Intercomparison results between AMSR2 and TMI/AMSR-E/GMI (AMSR2 Version 2.0)*. JAXA. Retrieved from https://suzaku.eorc.jaxa.jp/GCOM_W/materials/product/150326_AMSR2_XcalResults.pdf

Kenigson, J. S., & Timmermans, M.-L. (2021). Arctic cyclone activity and the Beaufort high. *Journal of Climate*, *34*, 4119–4127. https://doi.org/10.1175/JCLI-D-20-0771.1

Kern, S., Khvorostovsky, K., Skourup, H., Parsakhoo, Z. S., Parsakhoo, Z. S., Djepa, V., et al. (2015). The impact of snow depth, snow density and ice density on sea ice thickness retrieval from satellite radar altimetry: Results from the ESA-CCI sea ice ECV project round robin Exercise. *The Cryosphere*, *9*, 37–52. https://doi.org/10.5194/tc-9-37-2015

Kim, J. M., Sohn, B. J., Lee, S. M., Tonboe, R. T., Kang, E. J., & Kim, H. C. (2020). Differences between ICESat and CryoSat-2 sea ice thicknesses over the Arctic: Consequences for analyzing the ice volume trend. *Journal of Geophysical Research: Atmospheres*, *125*, e2020JD033103. https://doi.org/10.1029/2020JD033103

Koenig, L., Martin, S., Studinger, M., & Sonntag, J. (2010). Polar airborne observations fill gap in satellite data. *Eos Transaction American Geophysical Union*. *91*. 333–334. https://doi.org/10.1029/2010eo380002

Kurtz, N., & Harbeck, J. (2017). *CryoSat-2 Level-4 Sea Ice Elevation, Freeboard, and Thickness, Version 1*. Boulder, Colorado USA. NASA National Snow and Ice Data Center Distributed Active Archive Center. https://doi.org/10.5067/96JO0KIFDAS8

Kurtz, N., Studinger, M., Harbeck, J., Onana, V., & Yi, D. (2015). *IceBridge L4 Sea Ice Freeboard, Snow Depth, and Thickness, Version 1*. Boulder, Colorado USA: NASA National Snow and Ice Data Center. https://doi.org/10.5067/G519SHCKWQV6

Kurtz, N. T., & Farrell, S. L. (2011). Large-scale surveys of snow depth on Arctic sea ice from Operation IceBridge. *Geophysical Research Letters*, *38*, L20505. https://doi.org/10.1029/2011GL049216

Kurtz, N. T., Farrell, S. L., Studinger, M., Galin, N., Harbeck, J. P., Lindsay, R., et al. (2013). Sea ice thickness, freeboard, and snow depth products from Operation IceBridge airborne data. *The Cryosphere*, *7*, 1035–1056. https://doi.org/10.5194/tc-7-1035-2013

Kwok, R., & Cunningham, G. F. (2015). Variability of Arctic sea ice thickness and volume from CryoSat-2. *Philosophical Transactions of the Royal Society A*, *373*, 20140157. https://doi.org/10.1098/rsta.2014.0157

Kwok, R., Kacimi, S., Webster, M. A., Kurtz, N. T., & Petty, A. A. (2020). Arctic snow depth and sea ice thickness from ICESat-2 and CryoSat-2 freeboards: A first examination. *Journal of Geophysical Research: Oceans*, *125*, e2019JC016008. https://doi.org/10.1029/2019JC016008

Kwok, R., Kurtz, N. T., Brucker, L., Ivanoff, A., Newman, T., Farrell, S. L., et al. (2017). Intercomparison of snow depth retrievals over Arctic sea ice from radar data acquired by Operation IceBridge. *The Cryosphere*, *11*, 2571–2593. https://doi.org/10.5194/tc-11-2571-2017

Ledley, T. S. (1991). Snow on sea ice: Competing effects in shaping climate. *Journal of Geophysical Research*, *96*(D9), 17195–17208. https://doi.org/10.1029/91JD01439

Lee, S.-M., Meier, W. N., Sohn, B.-J., Shi, H., & Gasiewski, A. J. (2021). Estimation of Arctic basin-scale sea ice thickness from satellite passive microwave measurements. *IEEE Transactions on Geoscience and Remote Sensing*, *59*(7), 5841–5850. https://doi.org/10.1109/tgrs.2020.3026949

Lee, S.-M., & Sohn, B.-J. (2015). Retrieving the refractive index, emissivity, and surface temperature of polar sea ice from 6.9 GHz microwave measurements: A theoretical development. *Journal of Geophysical Research: Atmospheres*, *120*, 2293–2305. https://doi.org/10.1002/2014JD022481

Lee, S.-M., Sohn, B.-J., & Kim, S.-J. (2017). Differentiating between first-year and multiyear sea ice in the Arctic using microwave-retrieved ice emissivities. *Journal of Geophysical Research: Atmospheres*, *122*, 5097–5112. https://doi.org/10.1002/2016JD026275

Lee, S.-M., Sohn, B.-J., & Shi, H. (2018). Impact of ice surface and volume scatterings on the microwave sea ice apparent emissivity. *Journal of Geophysical Research: Atmospheres*, *123*, 9220–9237. https://doi.org/10.1029/2018JD028688

Lindsay, R., Wensnaham, M., Schweiger, A., & Zhang, J. (2013). Evaluation of seven different atmospheric reanalysis products in the Arctic. *Journal of Climate*, *27*(7), 2588–2606. https://doi.org/10.1175/JCLI-D-13-00014.1

Liston, G. E., Itkin, P., Stroeve, J., Tschudi, M., Stewart, J. S., Pedersen, S. H., et al. (2020). A Lagrangian snow-evolution system for sea-ice applications (SnowModel-LG): Part I—Model description. *Journal of Geophysical Research: Oceans*, *125*, e2019JC015913. https://doi.org/10.1029/2019JC015913

Markus, T., & Cavalieri, D. J. (1998). Snow depth distribution over sea ice in the Southern Ocean from satellite passive microwave data. *Antarctic Research Series*, *74*, 19–39. https://doi.org/10.1029/AR074p0019

Masunaga, H., Matsui, T., Tao, W., Hou, A. Y., Kummerow, C. D., Nakajima, T., et al. (2010). Satellite Data Simulator Unit: A multisensory, multispectral satellite simulator package. *Bulletin of the American Meteorological Society*, *91*, 1625–1632. https://doi.org/10.1175/2010BAMS2809.1

Maykut, G. A., & Untersteiner, N. (1971). Some results from a time-dependent thermodynamic model of sea ice. *Journal of Geophysical Research*, *76*(6), 1550–1575. https://doi.org/10.1029/JC076i006p01550

Meier, W. N., Fetterer, F., Savoie, M., Mallory, S., Duerr, R., & Stroeve, J. (2017). *NOAA/NSIDC Climate Data Record of Passive Microwave Sea Ice Concentration, Version 3*. Boulder, Colorado USA. NSIDC: National Snow and Ice Data Center. https://doi.org/10.7265/N59P2ZTG

Meier, W. N., Fetterer, F., & Windnagel, A. K. (2017). *Near-Real-Time NOAA/NSIDC Climate Data Record of Passive Microwave Sea Ice Concentration, Version 1*. Boulder, Colorado USA. NASA National Snow and Ice Data Center Distributed Active Archive Center. https://doi.org/10.7265/N5FF3QJ6

Petty, A. A., Kurtz, N. T., Kwok, R., Markus, T., & Neumann, T. A. (2020). Winter Arctic sea ice thickness from ICESat-2 freeboards. *Journal of Geophysical Research: Oceans*, *125*, e2019JC015764. https://doi.org/10.1029/2019JC015764

Petty, A. A., Kwok, R., Bagnardi, M., Ivanoff, A., Kurtz, N., Lee, J., et al. (2020). *ATLAS/ICESat-2 L3B Daily and Monthly Gridded Sea Ice Freeboard, Version 1*. Boulder, Colorado USA. NASA National Snow and Ice Data Center Distributed Active Archive Center. https://doi.org/10.5067/ATLAS/ATL20.001

Petty, A. A., Webster, M., Boisvert, L., & Markus, T. (2018). The NASA Eulerian Snow on Sea Ice Model (NESOSIM) v1.0: Initial model development and analysis. *Geoscientific Model Development*, *11*, 4577–4602. https://doi.org/10.5194/gmd-11-4577-2018

Ricker, R., Hendricks, S., Helm, V., Skourup, H., & Davidson, M. (2014). Sensitivity of CryoSat-2 Arctic sea-ice freeboard and thickness on radar-waveform interpretation. *The Cryosphere*, *8*, 1607–1622. https://doi.org/10.5194/tc-8-1607-2014

Rostosky, P., Spreen, G., Farrell, S. L., Frost, T., Heygster, G., & Melsheimer, C. (2018). Snow depth retrieval on Arctic sea ice from passive microwave radiometers–Improvements and extensions to multiyear ice using lower frequencies. *Journal of Geophysical Research: Oceans*, *123*, 7120–7138. https://doi.org/10.1029/2018JC014028

Serreze, M. C., Barrett, A. P., & Stroeve, J. (2012). Recent changes in tropospheric water vapor over the Arctic as assessed from radiosondes and atmospheric reanalyses. *Journal of Geophysical Research*, *117*, D10104. https://doi.org/10.1029/2011JD017421

Shi, H., Sohn, B.-J., Dybkjær, G., Tonboe, R. T., & Lee, S.-M. (2020). Simultaneous estimation of wintertime sea ice thickness and snow depth from space-borne freeboard measurements. *The Cryosphere*, *14*, 3761–3783. https://doi.org/10.5194/tc-14-3761-2020

Stroeve, J., Holland, M. M., Meier, W., Scambos, T., & Serreze, M. (2007). Arctic sea ice decline: Faster than forecast. *Geophysical Research Letters*, *34*, L09501. https://doi.org/10.1029/2007GL029703

Stroeve, J. C., Markus, T., Maslanik, J. A., Cavalieri, D. J., Gasiewski, A. J., Heinrichs, J. F., et al. (2006). Impact of surface roughness on AMSR-E sea ice products. *IEEE Transactions on Geoscience and Remote Sensing*, *44*(11), 3103–3117. https://doi.org/10.1109/TGRS.2006.880619

Tschudi, M., Meier, W. N., Stewart, J. S., Fowler, C., & Maslanik, J. (2019). *Polar Pathfinder Daily 25 km EASE-Grid Sea Ice Motion Vectors, Version 4*. Boulder, CO. NASA National Snow and Ice Data Center Distributed Active Archive Center. https://doi.org/10.5067/INAWUWO7QH7B

Wang, C., Graham, R. M., Wang, K., Gerland, S., & Granskog, M. A. (2019). Comparison of ERA5 and ERA-Interim near-surface air temperature, snowfall and precipitation over Arctic sea ice: Effects on sea ice thermodynamics and evolution. *The Cryosphere*, *13*, 1661–1679. https://doi.org/10.5194/tc-13-1661-2019

Warren, S. G., Rigor, I. G., Untersteiner, N., Radionov, V. F., Bryazgin, N. N., Aleksandrov, Y. I., & Colony, R. (1999). Snow depth on Arctic sea ice. *Journal of Climate*, *12*, 1814–1829. https://doi.org/10.1175/1520-0442(1999)012<1814:SDOASI>2.0.CO;2

Webster, M., Gerland, S., Holland, M., Hunke, E., Kwok, R., Lecomte, O., et al. (2018). Snow in the changing sea-ice systems. *Nature Climate Change*, *8*, 946–953. https://doi.org/10.1038/s41558-018-0286-7

Webster, M. A., Rigor, I. G., Nghiem, S. V., Kurtz, N. T., Farrell, S. L., Perovich, D. K., & Sturm, M. (2014). Interdecadal changes in snow depth on Arctic sea ice. *Journal of Geophysical Research: Oceans*, *119*, 5395–5406. https://doi.org/10.1002/2014JC009985

Yi, D., & Zwally, H. J. (2009). *Arctic Sea Ice Freeboard and Thickness, Version 1*. Boulder, Colorado USA, NASA National Snow and Ice Data Center Distributed Active Archive Center. https://doi.org/10.5067/SXJVJ3A2XIZT

Zhou, L., Stroeve, J., Xu, S., Petty, A., Tilling, R., Winstrup, M., et al. (2021). Inter-comparison of snow depth over Arctic sea ice from reanalysis reconstructions and satellite retrieval. *The Cryosphere*, *15*, 345–367. https://doi.org/10.5194/tc-15-345-2021

References From the Supporting Information

Alexandrov, V., Sandven, S., Wahlin, J., & Johannessen, O. M. (2010). The relation between sea ice thickness and freeboard in the Arctic. *The Cryosphere*, *4*, 373–380. https://doi.org/10.5194/tc-4-373-2010

Jutila, A., Hendricks, S., Ricker, R., von Albedyll, L., Krumpen, T., & Haas, C. (2021). Retrieval and parametrisation of sea-ice bulk density from airborne multi-sensor measurements. *The Cryosphere Discussion (in review)*. https://doi.org/10.5194/tc-2021-149

National Snow and Ice Data Center (NSIDC). (2004). *Morphometric Characteristics of Ice and Snow in the Arctic Basin: Aircraft Landing Observations from the Former Soviet Union, 1928-1989, Version 1*. Boulder, Colorado USA. NSIDC: National Snow and Ice Data Center. Compiled by Romanov, I. P. https://doi.org/10.7265/N5B8562T

Newman, T., Farrell, S. L., Richter-Menge, J., Elder, B., Connor, L., Kurtz, N., & McAdoo, D. (2014). Assessment of radar-derived snow depth measurements over Arctic sea ice. *Journal of Geophysical Research: Oceans*, *119*, 8578–8602. https://doi.org/10.1002/2014JC010284

Timco, G. W., & Frederking, R. M. W. (1996). A review of sea ice density. *Cold Regions Science and Technology*, *24*, 1–6. https://doi.org/10.1016/0165-232X(95)00007-X